ELECTRON CYCLOTRON EMISSION MEASUREMENTS DURING 28 GHz ELECTRON CYCLOTRON RESONANCE HEATING IN WENDELSTEIN WVII-A STELLARATOR

H.J. Hartfuß, U. Gasparino, M. Tutter

WII – A Team* , ECRH Group**

IPP 2/292 November 1987

MAX-PLANCK-INSTITUT FÜR PLASMAPHYSIK

8046 GARCHING BEI MÜNCHEN

MAX - PLANCK - INSTITUT FÜR PLASMAPHYSIK

GARCHING bei MÜNCHEN

ELECTRON CYCLOTRON EMISSION MEASUREMENTS DURING 28 GHz ELECTRON CYCLOTRON RESONANCE HEATING IN WENDELSTEIN WVII-A STELLARATOR

H.J. Hartfuß, U. Gasparino, M. Tutter

WII – A Team* , ECRH Group**

IPP 2/292 November 1987

* R. Brakel, G. Cattanei, D. Dorst, A. Elsner, K. Engelhardt, V. Erckmann, G. Grieger, P. Grigull, H. Hacker, H. Jäckel, R. Jaenicke, J. Junker, M. Kick, H. Kroiss, G. Kühner, H. Maaßberg, C. Mahn, G. Müller, W. Ohlendorf, F. Rau, H. Renner, H. Ringler, F. Sardei, A. Weller, H. Wobig, E. Würsching, M. Zippe

** W. Kasparek, G.A. Müller, E. Räuchle, P.G. Schüller, K. Schwörer, M. Thumm (Institut für Plasmaforschung der Universität Stuttgart)

Die nachstehende Arbeit wurde im Rahmen des Vertrages zwischen dem Max-Planck-Institut für Plasmaphysik und der Europäischen Atomgemeinschaft über die Zusammenarbeit auf dem Gebiete der Plasmaphysik durchgeführt

Abstract

Electron cyclotron emission measurements have been carried out on electron cyclotron resonance heated plasmas in the WENDELSTEIN VII-A Stellarator. Blackbody radiation from the thermalized plasma main body as well as radiation from a small amount of weakly relativistic suprathermal electrons has been detected. In addition sideband emission has been observed near the second harmonic of the heating line source. Harmonic generation and parametric wave decay at the upper hybrid layer may be a reasonable explanation.

1. Introduction

In the Wendelstein WVII-A Stellarator /1/ hot dense plasmas have been built up from the neutral gas by irradiating a linearly polarized intense millimeter wave in ordinary (O) mode orientation from the low field side of the torus (/2/, /3/). This report deals with early experiments conducted at 28 GHz corresponding to the first harmonic electron cyclotron frequency at a toroidal field of 1 T on the torus axis. Up to 200 kW from a gyrotron tube have been launched with a pulse length of 40 ms. More recent results are summarized in Refs. /4/,/5/.

About one half of the injected power contributes to the global plasma heating /2/. Absorption is localized in the region sorrounding the resonance layer where the local electron cyclotron frequency $\omega_{ce}(\underline{x})$ is equal to the frequency of the injected wave. The main contribution to absorption is expected to come from the first pass of the injected radiation through this layer.

Central electron temperature of 1.2 KeV has been obtained at a density of $5 \cdot 10^{18}\ m^{-3}$ corresponding to half the cut-off density at 28 GHz.

The ion temperature of the thermalized ion bulk is 100 to 150eV. But in addition a high energetic tail in the ion energy distribution is found corresponding to $300 \div 500\ eV$. A few per cent of the total amount of ions belong to this fast population (/6/,/7/).

The electron temperature and density reported are deduced from Thomson scattering measurements /8/. Besides electron cyclotron emission (ECE), measurements have been carried out to check the possibility of electron temperature evaluation by this diagnostic in the presence of the intense electron cyclotron resonance heating (ECRH) line source.

The single mode ECE power $kT_e \cdot \Delta f$ received from a plasma with 1 KeV electron temperature T_e within 1 GHz bandwidth Δf is about $2 \cdot 10^{-7}\ W$. Comparison with the gyrotron power launched at 28 Ghz, corresponding to the center of the ECE band, makes clear that no measurements at the first harmonic of the ECE, within close spectral neighbourhood to the strong line radiation, are possible. At the 2^{nd} harmonic,around 56 GHz, measurements of the electron cyclotron emission become possible by suppressing the fundamental gyrotron radiation in the receiver observation path with a high pass filter and the much weaker 2^{nd} harmonic emission of the gyrotron (1%) by a stop-band filter. In this way the 2^{nd} harmonic ECE is almost free of interference from the direct gyrotron emission.

Determination of electron temperature by ECE measurements is based on the assumption that the emitting plasma has reached a local thermodynamical equilibrium, so that a local temperature can be defined and the electron distribution function can be represented by means of a Maxwellian. Under this hypothesis the power emitted at an optically thick frequency is directly related, through the black-body radiation law, to the temperature at the point at which the emission

occurs. Calibration of the ECE radiometer makes use of this fact, so that the power detected is measured in terms of equivalent black-body temperature.

Spontaneous electron cyclotron emission occurs in a small frequency-band around the local electron cyclotron frequency:

$$\omega_{ce}(\underline{x}) = \frac{eB(\underline{x})}{m_e} \tag{1}$$

(e is the electron charge, $B(\underline{x})$ the magnetic field strength at the point $\underline{x}$ and m_e the electron mass). Relativistic "mass dependence" and Doppler effect are the two main physical mechanisms contributing to the broadening of the emission line. An electron with velocity $\underline{v}$ can interact with a wave characterized by the frequency ω and the parallel component (with respect to the external magnetic field) of the wave vector $k_{||}$ only if the "resonance relation":

$$\omega - k_{||}v_{||} - \frac{n\omega_{ce}(\underline{x})}{\gamma} = 0 \tag{2}$$

is satisfied. Here γ is the usual relativistic factor:

$$\gamma = \gamma(v) = \frac{1}{\sqrt{1 - \frac{v^2}{c^2}}}.$$

Using a semi-classical approach, Eq. (2) can be shown to be a consequence of conservation of energy and parallel momentum in the interaction between a photon and an electron in an uniform magnetic field.

The quality of the spatial resolution of the temperature profile derived from the ECE-spectrum depends on the bandwidth of the radiometer (see below) and on the possibility to relate the emitted frequency to the position at which such emission occurs. To increase the spatial resolution a minimization of line broadening effects is required. While the relativistic line broadening is a characteristic of the energy spread of the electron distribution function itself, Doppler broadening can usually be excluded by means of perpendicular observation (with respect to the toroidal magnetic field).

If the emitting plasma layer is not optically thick (grey or coloured emitter) the equivalent black-body radiation temperature, as measured by the radiometer, is not directly related to the physical temperature of the emitter, but it is still used as a measure of emitted intensity. If wall reflections are considered, the emitted power density approaches the black-body level; but if rays of equal frequency originating in plasma layers of different temperature are scrambled, the direct relation between emitted frequency and position of emission is lost.

Considering an electron temperature of 1.2 KeV and a density of $5 \cdot 10^{18}\ m^{-3}$, emission at the second harmonic is expected to be optically thick and can be used

to obtain information about the electron temperature profile. The aim of this report is to give a detailed description of the instrumentation and experimental observations in order to make the reader familiar with the difficulties and the way the conclusions are gained.

2. Instrumentation

In the range of 20 to 200 GHz the spectrum has been scanned using a fast (6 ms) Michelson interferometer /9/ with a He cooled InSb detector. This quasi-optical system does not contain the filters mentioned above, but a strong decrease in detector sensitivity below 45 GHz is inherent. This fact allows measurements close to the gyrotron frequency without further protection. However, due to the strong intensity fluctuations of the signals received during the ECR- heated discharges, no reproducible spectra could be obtained from a single scan. Averaging of a large number of interferograms taken during a series of shots was necessary to obtain spectra sufficiently free of noise.

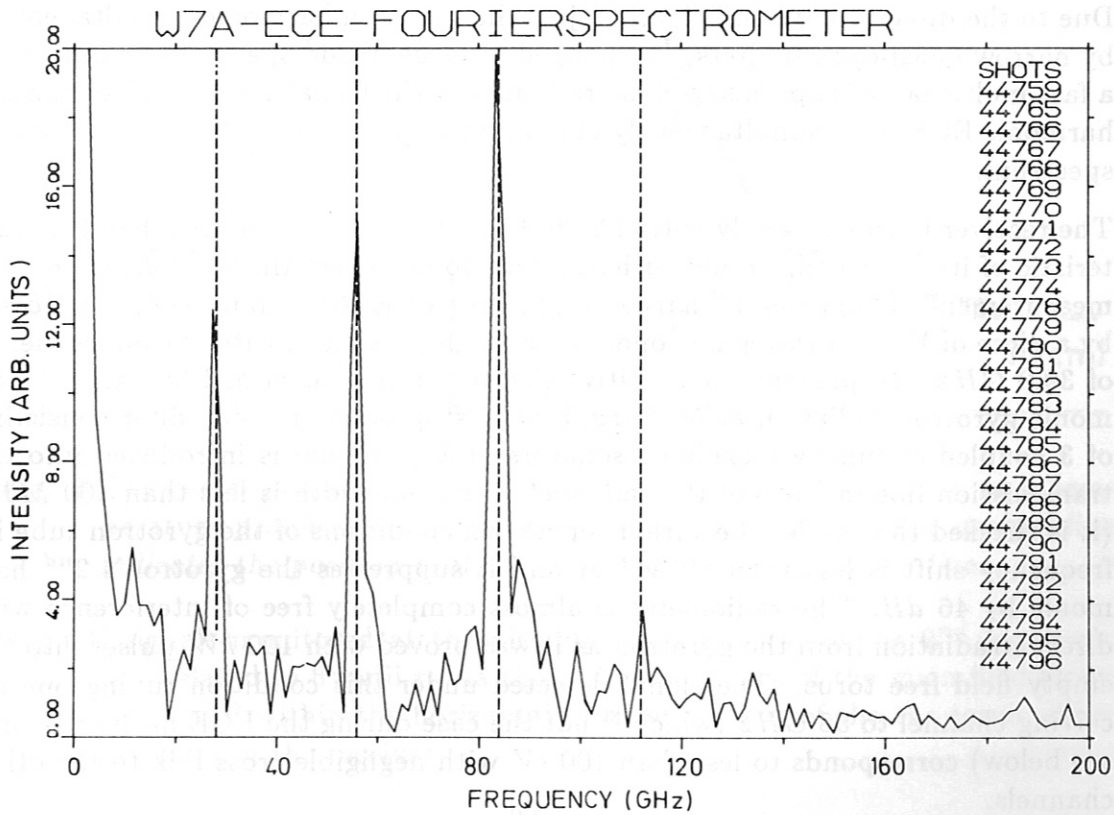

Fig.1 The spectrum of the gyrotron radiation measured by a fast scanning Michelson interferometer with subsequent Fourier transform. 30 measurements have been averaged.

The result averaging 30 spectra after Fourier inversion of the interferograms is given in Fig. 1. Four lines are resolved whose frequencies correspond to the 1^{st} to 4^{th} harmonic of the gyrotron radiation frequency. The linewidth is clearly smaller than the expected bandwidth of the ECE spectrum. It corresponds to the

resolution of the Michelson interferometer.

The spectrum as given in Fig. 1 is not corrected for the frequency dependent overall sensitivity of the instrument. But an estimation of the received power within the 56 GHz line results in about 800 times the ECE power which would be received under the same experimental conditions from a plasma with 1 KeV electron temperature.

We conclude that the observed spectrum is the spectrum of the gyrotron tube itself. The strong fluctuations are due to fluctuating absorption and reflection of the primary beam by the plasma (fluctuations of the same character are seen in the reflected gyrotron power). The fluctuations generate a high noise level in the Fourier-spectogram which completely covers the ECE bands.

Due to the difficulties to sufficiently reject the gyrotron harmonics simultaneously by narrow quasi-optical filters, we changed to single mode operation and installed a fast multichannel superheterodyne radiometer which enables to monitor the 2^{nd} harmonic ECE band simultaneously at 8 discrete frequencies within its continuous spectrum.

The receiver is sensitive only within 50 to 60 GHz due to the narrow band characteristic of its front end. So higher harmonics do not affect the 2^{nd} harmonic ECE measurement. The strong 1^{st} harmonic gyrotron emission is completely suppressed by a piece of V-band waveguide operated as high pass filter, with cut-off frequency of 39.9 GHz. To prevent the sensitive electronics from overload by the 2^{nd} harmonic gyrotron radiation at 56 GHz, a deep stop-band or notch filter consisting of 3 coupled circular waveguide resonators (TE_{111} mode) is introduced into the transmission line in front of the radiometer. Its halfwidth is less than 100 MHz (it is checked that under the various operation conditions of the gyrotron tube its frequency shift is less than 50 MHz) and it suppresses the gyrotron's 2^{nd} harmonic by 46 dB. The radiometer is almost completely free of interference with direct irradiation from the gyrotron as it was proved with 100 kW pulses into the empty field free torus. The signal detected under this condition tuning one receiving channel to 56 GHz (which is not the case during the ECE measurements, see below) corresponds to less than 100 eV with negligible cross talk to the other channels.

The multichannel radiometer, /10/, works as follows: the 5 to 6 GHz wide 2^{nd} harmonic ECE band centered at 56 GHz is downconverted to a wideband intermediate frequency (IF) using a 63.52 GHz local oscillator frequency. The IF band ranges from 5 to 10.04 GHz. After amplification the signal path is split into 8 different channels each containing a 300 MHz wide band-pass filter. The center frequencies of these filters differ by 720 MHz. After passing the individual filters, the signals are rectified by a square law detector and fed into the general WVII-A CAMAC system. In this way the ECE spectrum is monitored at 8 channels. The radiometer channels are absolutely calibrated by comparison with a black-body of

well known temperature applying the hot-cold technique. Signal strength is given in terms of equivalent blackbody temperature.

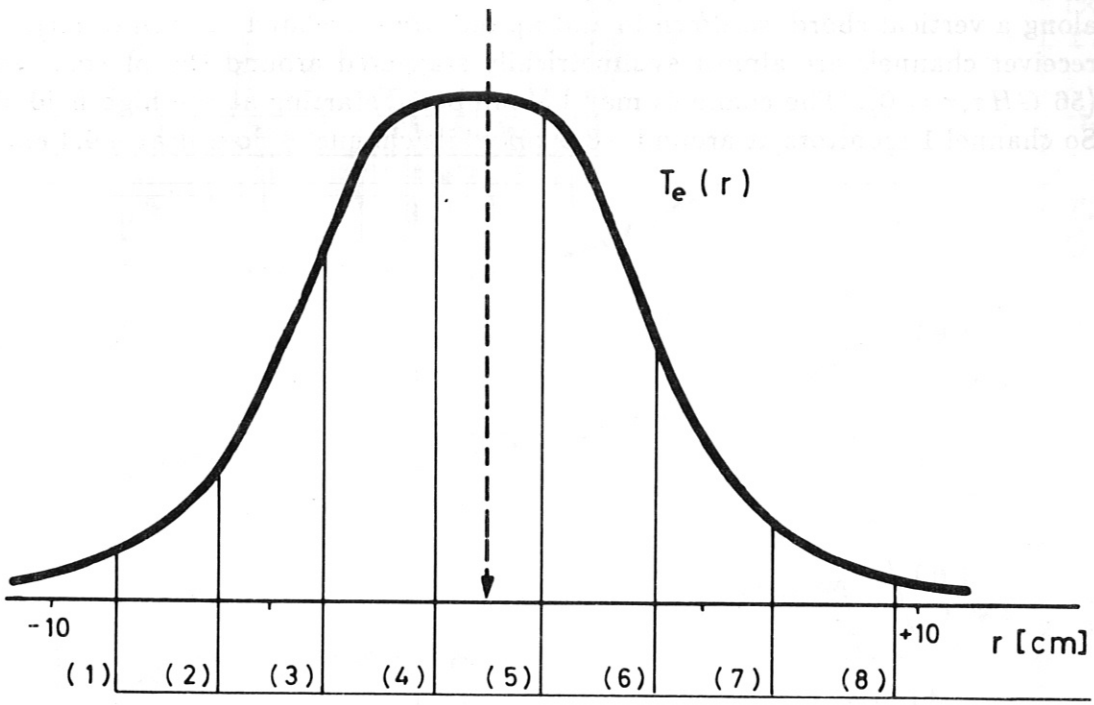

Fig. 2 The radial positions of the 8 radiometer channels in relation to a temperature profile as measured by Thomson scattering. The dashed line indicates the position of the 2^{nd} harmonic of the gyrotron line.

The ECE signals monitored at the discrete frequencies f_i of the 2^{nd} harmonic emission, are related to 8 radii r_i via the $1/R$ dependence of the main field along the major radius R within the horizontal symmetry plane of the the torus which is the line of sight of the receiver

$$r_i = R_0 \frac{2f_0 - f_i}{f_i} \quad , \tag{3}$$

where

$$R_0 = \text{major radius} = 2\ m \quad ,$$

$$f_0 = \frac{1}{2\pi}\frac{e}{m} B(R_0) = 28\ GHz$$

$$f_i = f(R_0 + r_i)$$

$$B(R_0) = \text{main field on torus axis.}$$

The 300 MHz bandwidth Δf of each observation channel corresponds to a plasma layer thickness of $\Delta r \simeq R_0 \cdot (\Delta f / f_0) = 200 \cdot (0.3/56)\ cm = 1.1\ cm$, while the "distance" of the channels is 2.6 cm.

Fig. 2 gives the radial positions in relation to an electron temperature profile as measured by Thomson scattering. (Note that this profile is obtained viewing along a vertical chord, so down-in and up-out are correlated to each other). The receiver channels are almost symmetrically staggered around the plasma center (56 $GHz, r = 0$). The channels may be numbered starting at the high field side. So channel 1 monitors at around $-8.6\ cm$ while channel 8 does it at $+9.4\ cm$.

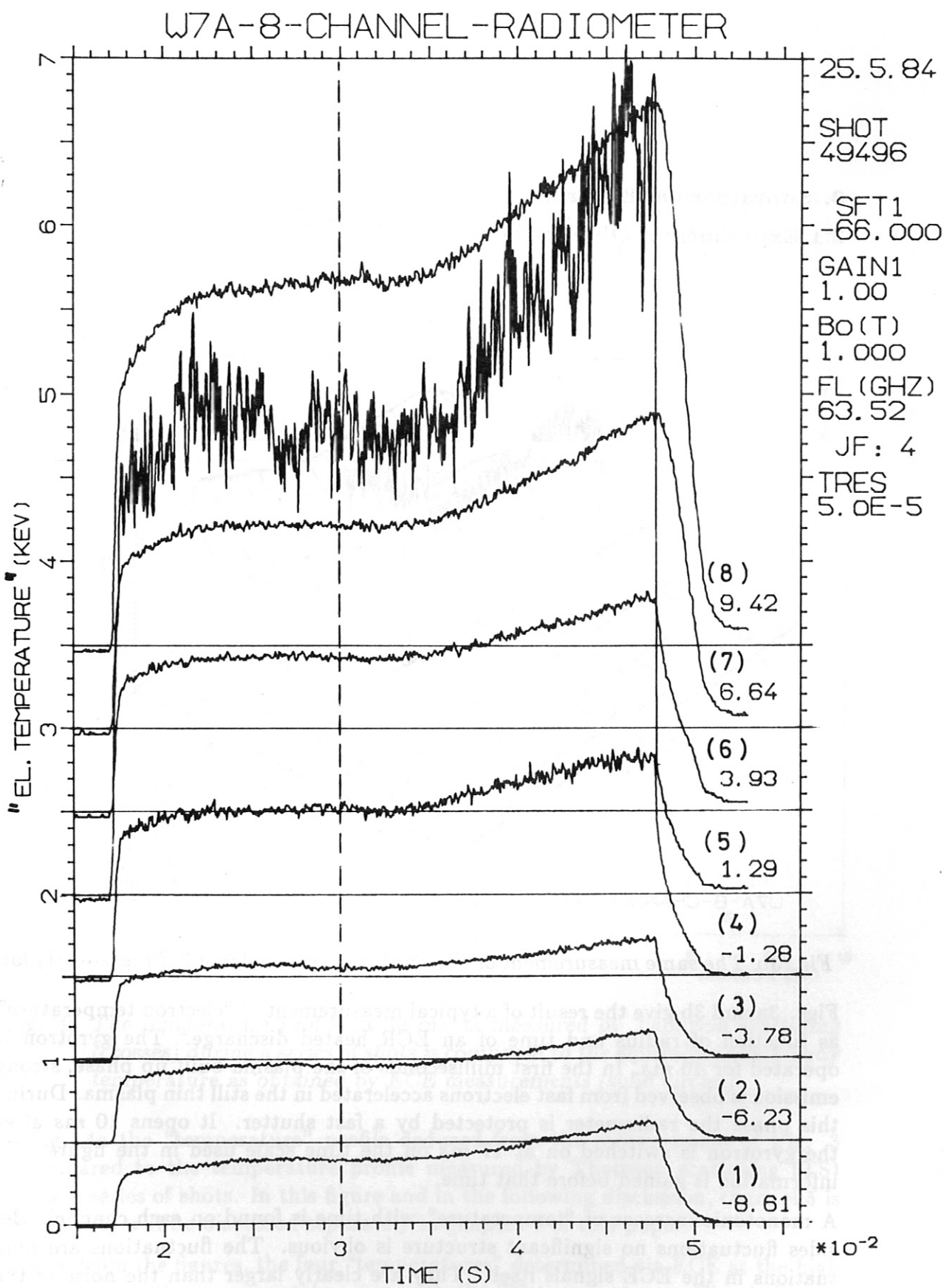

Fig. 3a The power in terms of equivalent blackbody temperature as detected by the radiometer channels (1) to (8) as function of time for a typical ECRH heated discharge. The numbers below the channel number (n) give the mean position in cm for the individual channels. Note that subsequent traces are shifted upwards by 0.5 KeV

3. Suprathermal Electrons

3.1 Experimental Observations

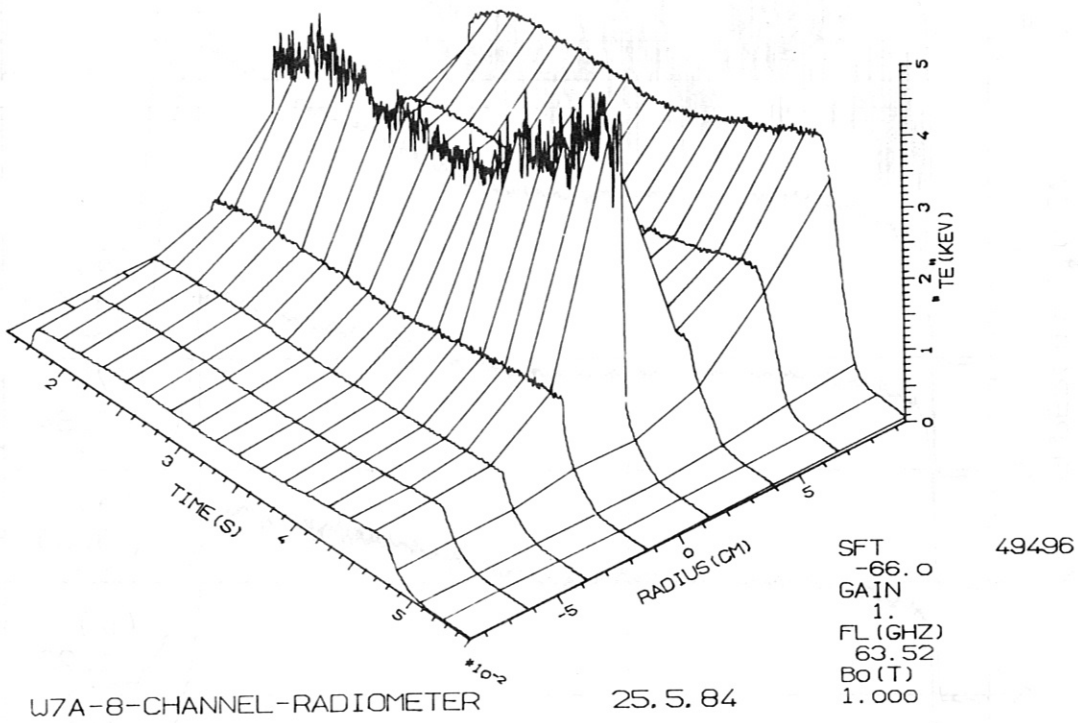

Fig. 3b The same measurement of Fig. 3a here presented in a 3-dimensional plot.

Figs. 3a and 3b give the result of a typical measurement of "electron temperature" as function of radius and time of an ECR heated discharge. The gyrotron is operated for 40 *ms*. In the first milliseconds of the plasma built up phase, strong emission is observed from fast electrons accelerated in the still thin plasma. During this phase the radiometer is protected by a fast shutter. It opens 10 *ms* after the gyrotron is switched on at 17 *ms* on the time scale used in the figure. No information is gained before that time.

A monotonic increase of "temperature" with time is found on each channel. Besides fluctuations no significant structure is obvious. The fluctuations are fluctuations in the ECE signals itself. They are clearly larger than the noise of the radiometer. Channel 5 deviates in that it shows much stronger fluctuations than the other channels.

The shape of the profile of Fig. 3b is completely different from what expected. Only the 4 inner channels 1 to 4 on the high field side are close to the expec-

tations,i.e., monotonic increase of the "temperature" towards the plasma center. Channel 5 deviates again strongly, rising to much larger signal amplitude than its neighbour channels. Channels 6 to 8 should correspond to an increasing "temperature" up to 3 KeV at the outer plasma boundary.

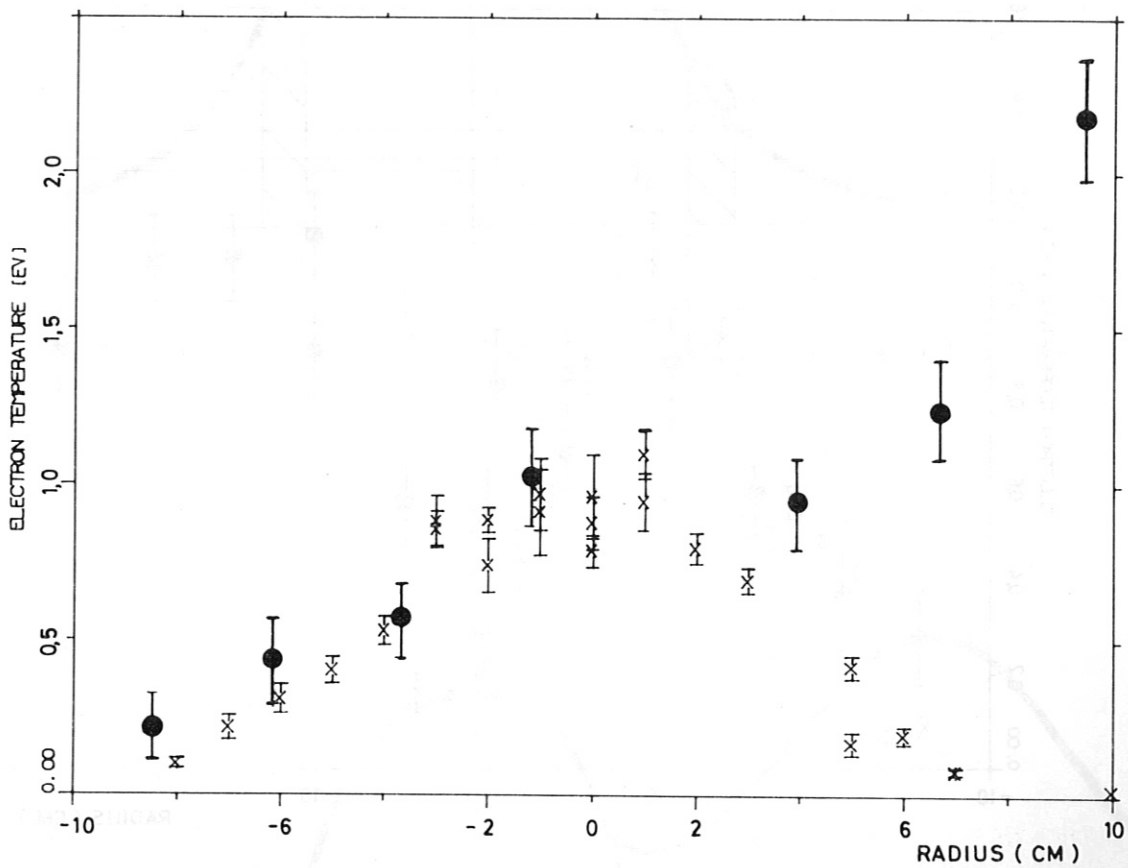

Fig. 4a The temperature profile at 30 ms as measured by Thomson scattering (crosses) during a series of shots is compared to the equivalent black-body temperature as obtained by ECE measurements (solid circles)

In Fig. 4a the "temperature" profile deduced from the measurement of Fig. 3 is compared to the temperature profile measured by Thomson scattering (TS) during a series of shots. In this figure and in the following discussion, channel 5 is removed. It will be discussed separately in chapter 4 of this paper.
As seen from the figures, the four "temperatures" determined via ECE at the high field side ($r < 0$) approximately agree with the TS temperatures. This indicates that the four plasma layers monitored indeed behave like blackbody emitters, i.e., the equivalent blackbody temperatures correspond to the electron temperatures at these radii. On the low field side ($r > 0$) the emitted power is found to increase with the minor radius instead of decreasing. This is true for each of the measurements

in a series of shots. The slope at larger radii ($r > 10\ cm$) has been determined by slightly increasing the main magnetic field, shifting the receiving channels to larger radii. As a consequence the resonance zone for ECR power absorption is shifted too. Therefore, the shots slightly differ from each other.

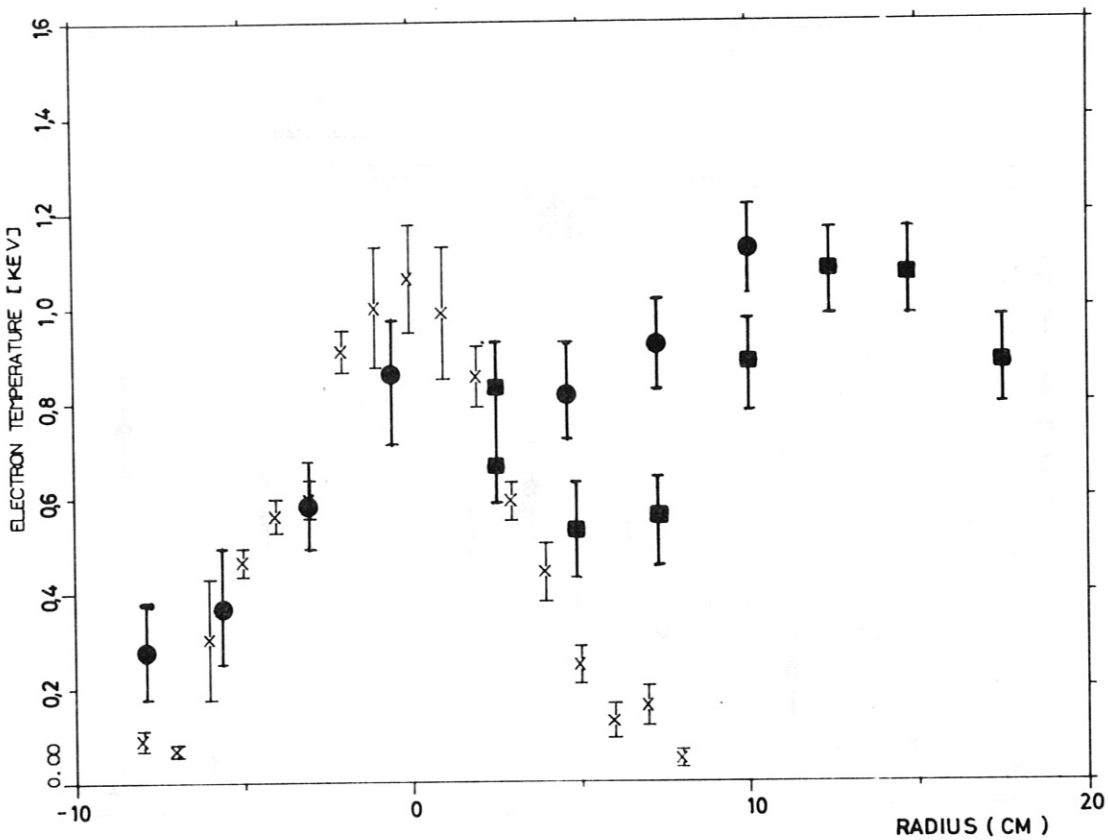

Fig. 4b "Electron temperature" deduced from ECE measurements (solid circles) in comparison to the electron temperature profile measured by Thomson scattering (crosses). The solid squares are obtained by reducing the main magnetic field by about 3%.

Nevertheless, the essential feature may be deduced from Fig. 4b which gives the temperature profile on an extended scale. An additional broad maximum is found around $r = 13\ cm$. This indicates that the frequency to radius conversion via Eq. (2) is not valid: $r = 13\ cm$ is clearly outside the last closed flux surface of the WVII-A Stellarator for $B = 1\ T, \iota = 0.6$.

The observation can be explained assuming a certain amount of weakly relativistic suprathermal electrons. In this case the cyclotron frequency is shifted towards lower frequencies according to Eq. (2) (viewing the antenna in a plane nearly perpendicular to the main magnetic field, $k_{||}$ is a small quantity and the Doppler

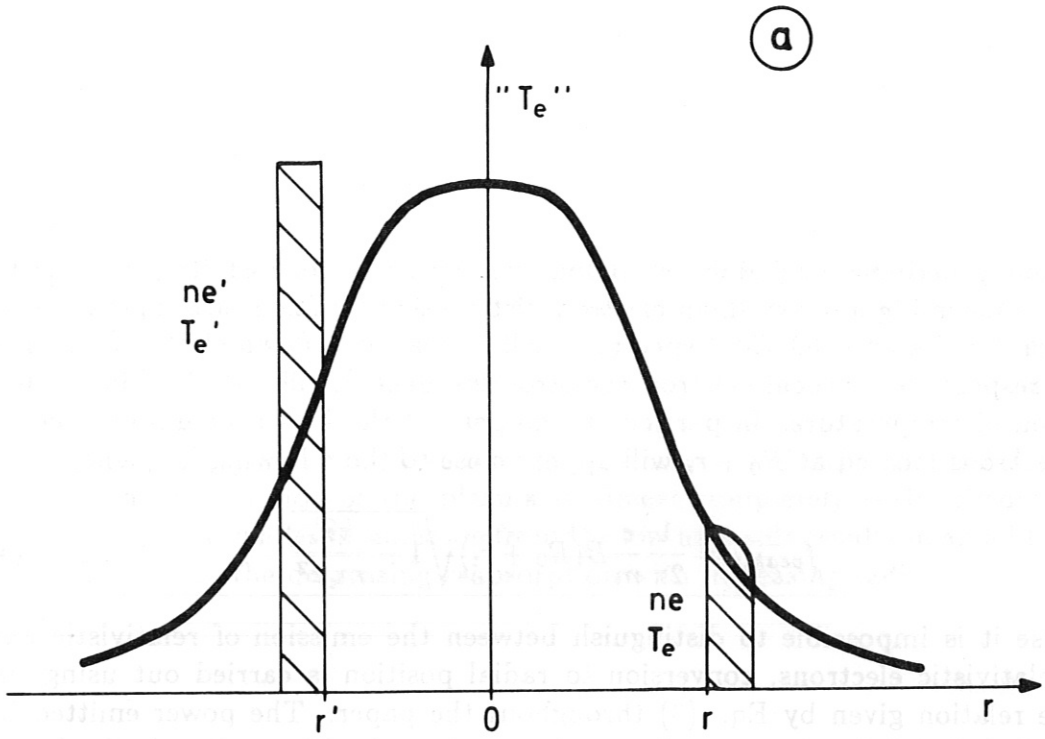

Fig. 5a A thin layer with suprathermal population at r' may cause a slight profile change at r.

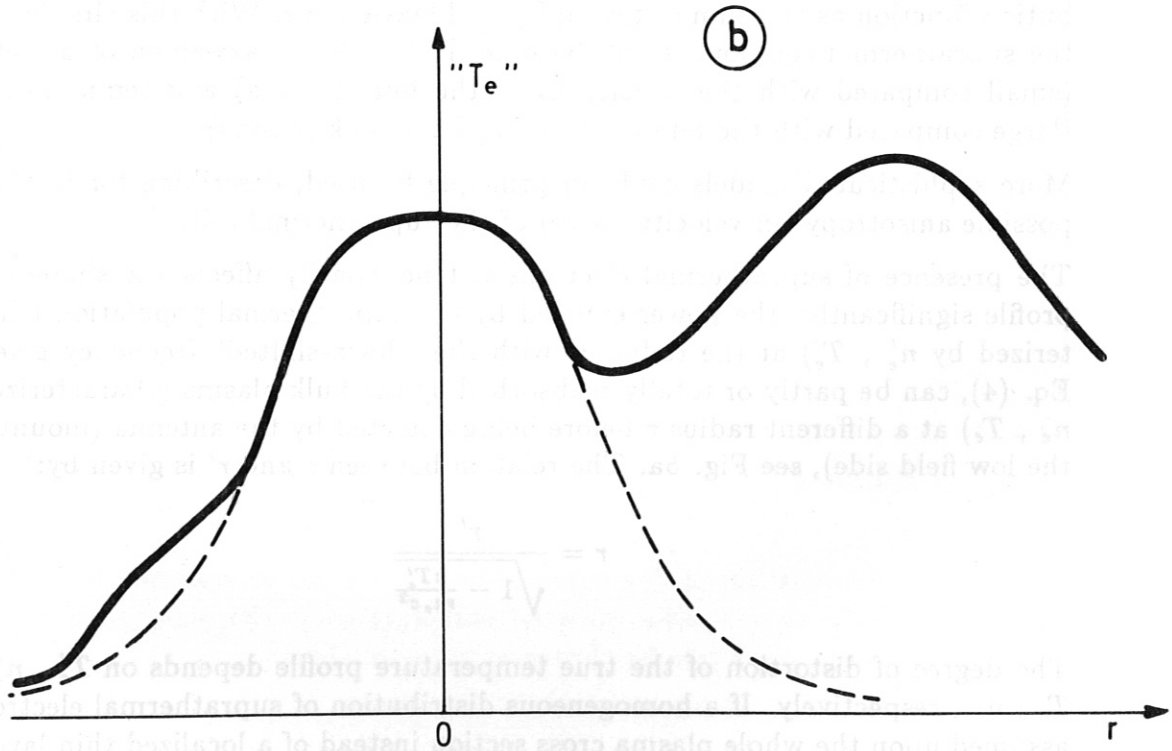

Fig. 5b A homogeneous distribution of suprathermal electrons upon the whole plasma cross section may lead to an apparent "temperature profile" as shown in this figure.

broadening becomes negligible in comparison with the down-shifting relativistic effect). Assuming a Maxwellian electron distribution function of temperature T_e the peak of the emitted ECE spectrum will appear at a down-shifted frequency (with respect to the local electron cyclotron frequency). The shifting factor is a function of temperature. In particular, the peak of the EC-spectrum emitted by the electrons located at $R_0 + r_i$ will appear close to the following frequency:

$$f_{peak,i} = \frac{1}{2\pi}\frac{e}{m}B(R_0 + r_i)\sqrt{1 - \frac{kT_e}{m_e c^2}} \tag{4}$$

Because it is impossible to distinguish between the emission of relativistic and non-relativistic electrons, conversion to radial position is carried out using the simple relation given by Eq. (3) throughout the paper. The power emitted by a weakly relativistic electron tail superimposed to the Maxwellian bulk plasma component will be therefore correlated with too large radii. This shift is about 2 cm for electrons with an average energy of 10 KeV.

The simplest theoretical model to describe the presence of a suprathermal component superimposed to the Maxwellian background is to write the electron distribution function as the sum of two different Maxwellians. With this simple model the suprathermal component will be described with a Maxwellian of density n'_e (small compared with the density n_e of the bulk plasma) and temperature T'_e (large compared with the temperature T_e of the bulk plasma).

More sophisticated models could in principle be used, describing for instance a possible anisotropy (in velocity space) of the suprathermal tail.

The presence of suprathermal electrons not necessarily affects the shape of the profile significantly: the power emitted by the suprathermal population (characterized by n'_e , T'_e) at the radius r' with the "down-shifted" frequency given by Eq. (4), can be partly or totally reabsorbed by the bulk plasma (characterized by n_e , T_e) at a different radius r before being detected by the antenna (mounted at the low field side), see Fig. 5a. The relation between r and r' is given by:

$$r = \frac{r'}{\sqrt{1 - \frac{kT'_e}{m_e c^2}}} \tag{5}$$

The degree of distortion of the true temperature profile depends on T'_e , n'_e and T_e , n_e , respectively. If a homogeneous distribution of suprathermal electrons is assumed upon the whole plasma cross section instead of a localized thin layer, an apparent "temperature" profile, as the one given in Fig. 5b, is expected.

Being the antenna installed at the outer side of the torus, the power emitted at a down-shifted frequency by the suprathermal component has to pass through the layer where the thermal electrons are resonant, before being detected. For frequencies at which the thermal resonance is optically thick, the incoming radiation

can be totally reabsorbed and the emitted power still be related, throught the black-body emission law, to the bulk temperature at the thermal resonance. For frequencies at which the thermal resonance is not optically thick the incoming radiation cannot be considerably reabsorbed and the power received at the antenna will be the superposition of radiation emitted by particles, of different energy, at different position. The examples show that the emission of suprathermal electrons from the high field side of the plasma is almost completely reabsorbed by the thermalized bulk, while the emission from the low field side results in an additional maximum due to the decreasing reabsorption with increasing radii.

3.2 Numerical Simulation

Numerical calculations have been carried out to simulate the observed spectra. We used the most simple approach to the problem, calculating the temperature profile as seen by a single ray along the major radius R through the plasma column. The basis of the 1-dimensional simulations is the electron temperature and density profile as measured by the Thomson scattering diagnostic, from which the optical depth $\tau(R)$ of the thermal bulk for the 2^{nd} harmonic ECE in X-mode and the emittance $(1 - e^{-\tau(R)})$ can be calculated /11/. The emission profile is derived dividing the plasma column into a large number of thin layers considering $\tau = \tau(R)$ and folding with the Doppler profile of each single layer. With the increase of the optical depth, $\tau \geq 4$, the emission is restricted to the outer surface of the emitting layers. This effect shifts the temperature profile as measured by ECE inwards to smaller R. Relativistic change of mass and the diamagnetic properties of the plasma, on the contrary, lead to an apparent outward shift. Usually the latter effects dominate resulting in an overall outward shift of the maximum and a slight asymmetry, characterized by a steepening of the shape at the outer edge and a flattening at the inside. In addition, the dielectric properties of the cold plasma passed by the ray are considered when calculating the temperature profile of the thermalized bulk.

Concerning the suprathermal component, it is assumed that its density is sufficiently low so that its self-reabsorption can completely be neglected. The emission has been calculated with the single particle radiation (Schott-Trubnikov) formula /12/. A suprathermal component with energy dependence of the form e^{-E/E_0} and minimum threshold value E_{c0} is thought to be superimposed to the Maxwellian background. Furthermore, all these suprathermal electrons are assumed to have the same pitch angle θ (angle between the electron velocity and the external magnetic field). Under these assumptions, the resulting emission spectrum is evaluated for each plasma layer /13/. On the way to the observer the radiation is partly reabsorbed $(e^{-\tau})$ at the cyclotron resonance layer (see Eq. (4)) by the thermal plasma as discussed above. Finally the emission spectra modified in this way are integrated over all the layers along the line of sight.

The density distribution of the suprathermal electrons is assumed to be homogeneous along the chord and symmetric with respect to the plasma axis between $\pm r_a$, but it can, in principle, be chosen arbitrarily /14/.

The results are given in Figs. 6a and 6b. The dashed curves are the slightly oblique temperature profiles corresponding to the thermalized bulk as they would be measured by ECE. The basis for the calculation are the symmetric TS temperature profiles of Figs. 4a and 4b. The solid curves are the "profiles" as seen by the ECE diagnostic if a small amount of suprathermal electrons is present. They are the best fit to the measured points that have been found by visual inspection and variation of the parameter E_0, E_{c0}, r_a and the suprathermal density. For perpen-

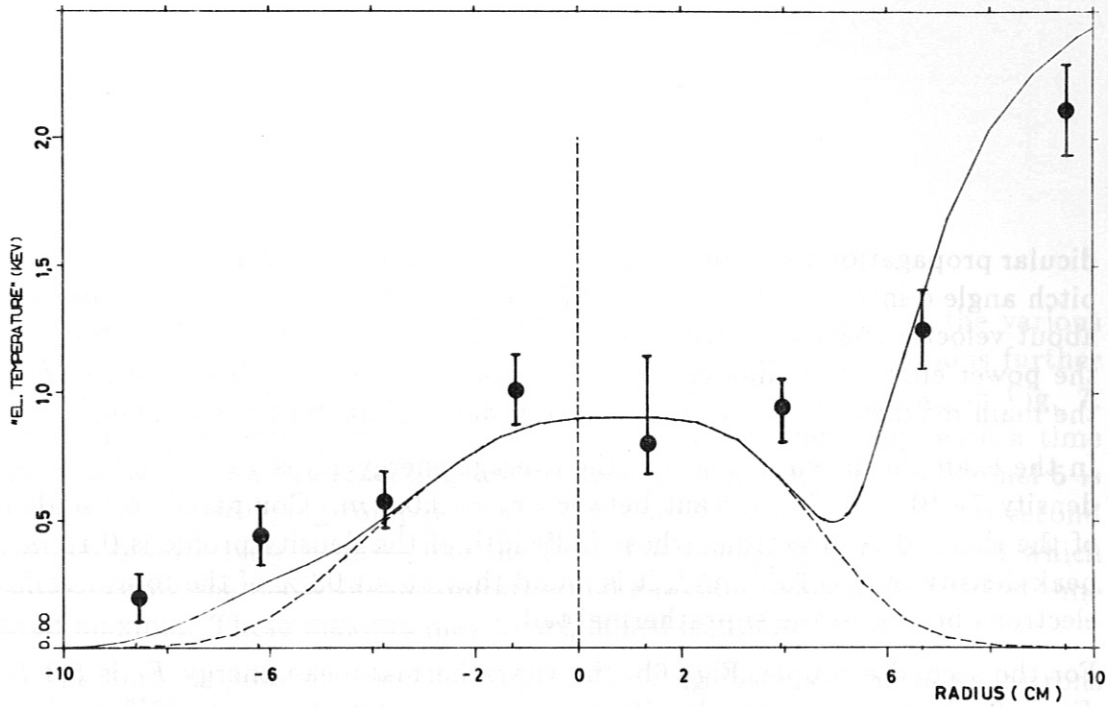

Fig. 6a The temperature profile as would be measured by ECE if no suprathermal population was present is given by the dashed line. Solid line refers to the best fit to the measured point in the framework of the 1-dimensional simulation. In addition to the thermal bulk a suprathermal population is assumed homogeneously distributed between ± 0.1 m with density $7 \cdot 10^{15}$ m^{-3} and average energy 10 KeV. The measurements as given in Fig. 4a are taken as the basis.

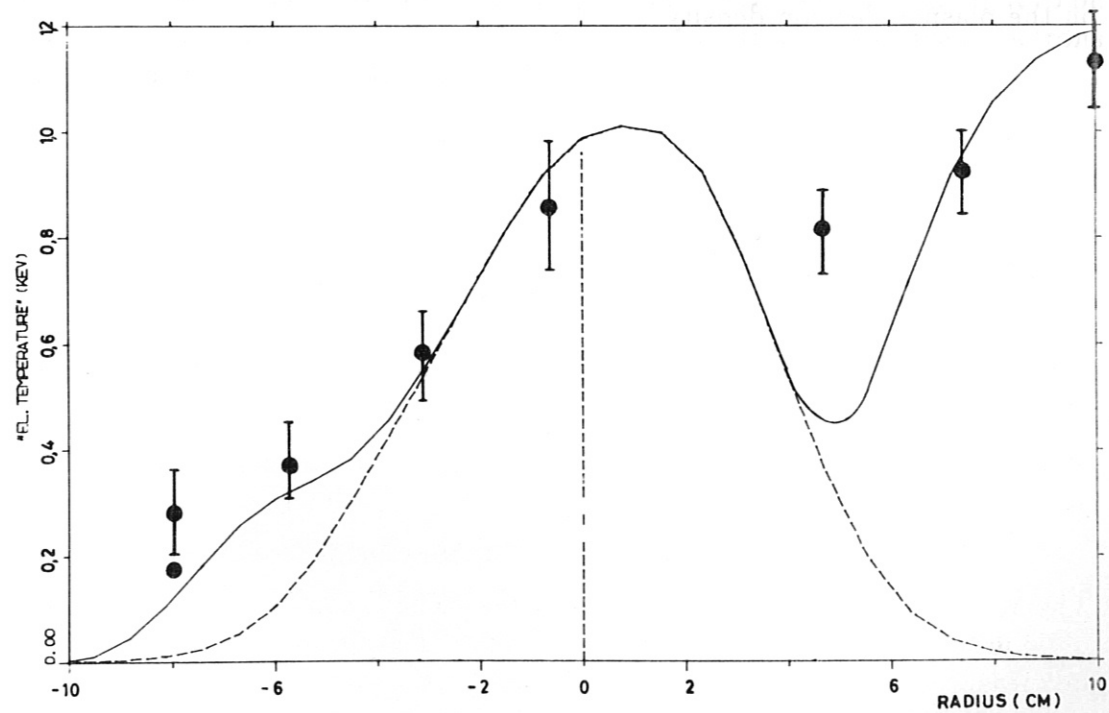

Fig. 6b Same as in Fig. 6a, but with the measurements of Fig. 4b as basis for the simulation. The best fit is obtained assuming an electron density of $1 \cdot 10^{16}$ m^{-3} homogeneously distributed between ± 0.1 m with average energy of 5.3 KeV.

dicular propagation the emitted spectrum is nearly independent on the value of the pitch angle θ introduced with the model of the distribution function. Information about velocity space anisotropy could, in principle, be obtained from the ratio of the power emitted at different harmonics or observing obliquely, with respect to the main magnetic field. No experimental data of this type are available.

In the example shown in Fig. 6a, the average energy E_0 is 10 KeV, $E_{c0} = 0$, the density $7 \cdot 10^{15}$ m^{-3}, constant between $r_a = \pm 0.1$ m. Compared to the density of the thermalized electrons whose halfwidth of the density profile is 0.11 m at a peak density of $5.8 \cdot 10^{18}$ m^{-3}, it is found that about 0.2% of the total number of electrons belong to the suprathermal tail.

For the second example, Fig. 6b, the suprathermal mean energy E_0 is 5.3 KeV, $E_{c0} = 0$, the homogeneous density again between ± 0.10 m, is $1 \cdot 10^{16}$ m^{-3} corresponding to about 0.3% of the total amount of electrons.

Better agreement with the eight measured "temperatures" of each example can be obtained modifying the density profile of the suprathermal population. But in the framework of a simple 1-dimensional model , an increasing number of fit parameters does not lead to more insight and confidence. So we restrict ourselves to the most simple assumptions concerning energy and density distribution. But we believe that the order of magnitude is correct, i.e. about 0.3% of a suprathermal component at an energy between 5 and 15 KeV. Both quantities strongly depend on the plasma electron density.

3.3 "Temperature" Decay

After the gyrotron is switched off, evaluation of the signal decay at the various channels confirms the ideas discussed so far and, in addition, it contains further information. The transient behaviour between 45 and 55 ms is shown in Fig. 7. The four high field side channels 1 to 4 decay purely exponentially, with a time constant of about 1.5 ms reflecting the electron confinement time. Channel 5 is composed of two decaying components: a fast one discussed below and a second one which qualitatively behaves like the three low field neighbours 6 to 8 which are governed by the decay of the suprathermal emission rising to additional time delayed maxima. These maxima may be explained as follows.

After the heating power is switched off, the driving force for the fast electrons disappears, resulting in a slowing-down process which decreases the relativistic electron mass and increases the emitted cyclotron frequency. As a result, the emission spectrum shrinks to the (decaying) thermal bulk, the low field side maximum is shifted inwards and its amplitude decreases while more and more fast electrons are lost.

This decay process can be simulated too, but because of the many free parameters involved, the persuasive force is restricted.

It should be noted that the decay and the whole transient behaviour, as observed by channel 8 , is very similar to the decay of the plasma current, which is thought to be composed of non-balanced toroidal currents carried by fast wave-driven electrons (no ohmic heating is used in this type of discharges).

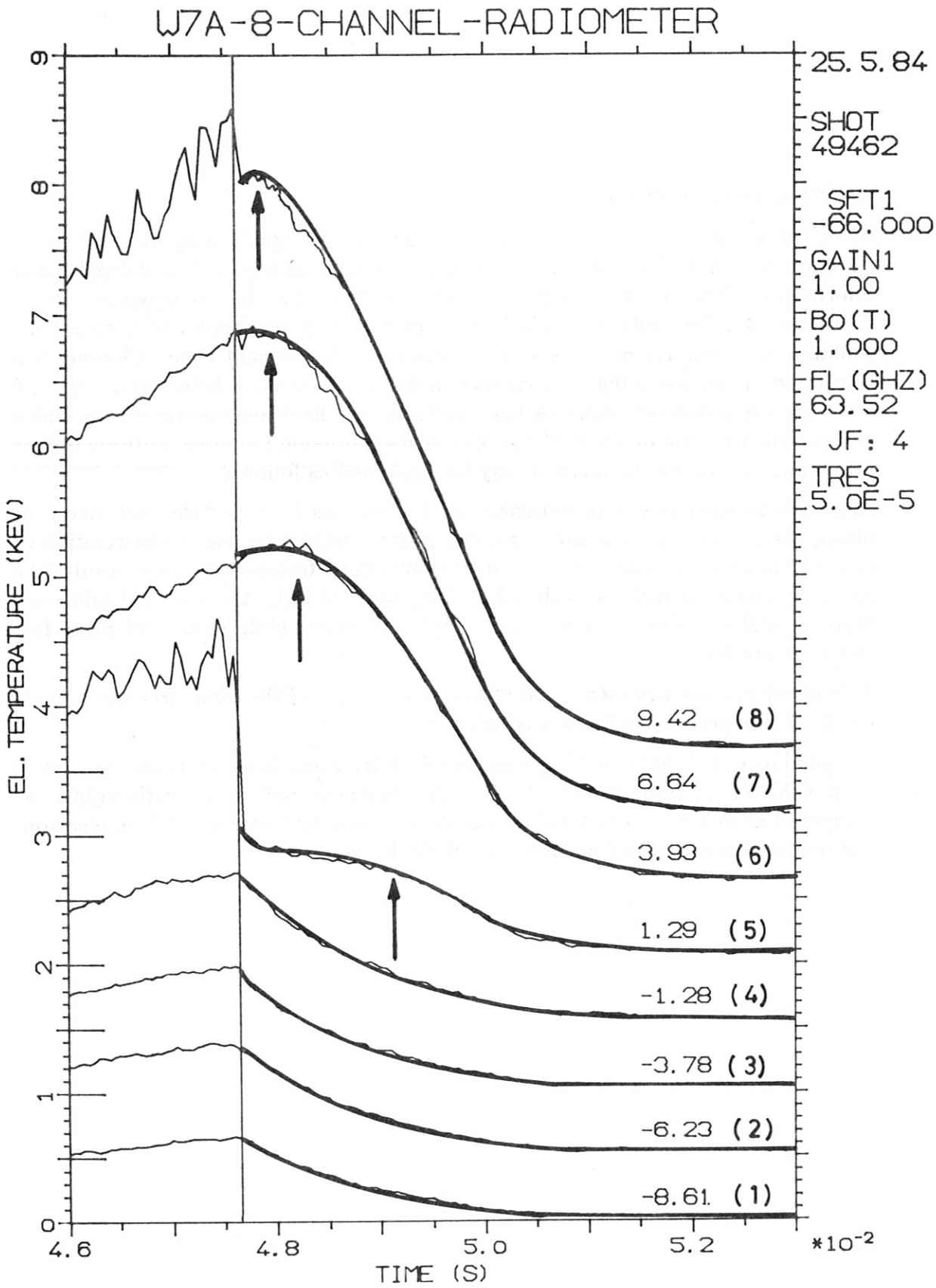

Fig. 7 The temporal decay of the "temperature" as measured at the eight positions as given in the figure. Additional time delayed maxima are found reflecting the slowing down process of the suprathermal population.

4. Sideband Emission

As pointed out in the introduction, the ECR heating power is launched along a major radius of the WVII-A torus from the low field side as a linearly polarized millimeter wave beam corresponding to the ordinary (O) wave polarization in the plasma, $k \perp B$, $E \parallel B$.

A small amount of the beam which has not been absorbed in the cyclotron resonance layer, penetrates the plasma column and is reflected by a focusing polarization twist reflector mounted on the inner wall of the torus. The reflected wave enters the plasma in extraordinary (X) mode polarization, $k \perp B$, $E \perp B$ and is partly absorbed in the electron cyclotron resonance zone.

When the upper hybrid layer, defined by $\omega^2 = \omega_{pe}^2 + \omega_{ce}^2$ and located at about 7 to 8 cm out of the plasma axis is reached, wave energy can be converted into upper hybrid oscillations of high amplitudes and nonlinear phenomena may arise. The incoming X wave (ω, k) can decay parametrically into an electron Bernstein mode (ω_1, k_1) and a lower hybrid wave (ω_2, k_2) conserving energy and momentum /15/.

$$\hbar\omega(k) = \hbar\omega_1(k_1) + \hbar\omega_2(k_2) \tag{6}$$

$$\hbar\underline{k} = \hbar\underline{k}_1 + \hbar\underline{k}_2 \tag{7}$$

The dispersion relations for the electron mode and the ion mode are approximately given by /16/:

$$\omega_1^2 \simeq \omega_{pe}^2 \cdot (1 - k_1^2 r_g^2) + \omega_{ce}^2 \tag{8a}$$

$$\omega_2^2 \simeq \omega_{lh}^2 \cdot (1 - k_2^2 r_g^2 \cdot \delta) \tag{8b}$$

where r_g is the gyroradius and $\delta = \delta(T_i, T_e, \omega_{ci}, \omega_{ce})$ is a function of the local parameters and is of order one.

So the frequencies of the decay waves are expected slightly below the upper hybrid frequency (which is identical to the X-mode pump frequency), and slightly above the lower hybrid frequency ω_{lh}. Considering the well known X-mode cold plasma dispersion relation as given by Appleton-Hartree /17/

$$(\frac{ck}{\omega})^2 = 1 - \frac{\omega_{pe}^2}{\omega^2} \cdot \frac{\omega^2 - \omega_{pe}^2}{\omega^2 - \omega_{pe}^2 - \omega_{ce}^2} \quad , \tag{9}$$

the decay process can schematically be sketched in an (ω, k)-diagram as in Fig. 8. In addition to the "Stokes" line ω_1 a weaker "anti Stokes" line ω_3 is expected above the pump frequency ω according to the process /18/

$$\hbar\omega(k) + \hbar\omega_2(k_2) = \hbar\omega_3(k + k_1) \tag{10}$$

Due to the finite width of the upper hybrid layer and due to the fact that a band of (ω_1, k_1) and (ω_2, k_1) exist into which the pump wave (ω, k) can decay, frequency bands are expected around $\omega_1, \omega_2, \omega_3$ rather than discrete lines.

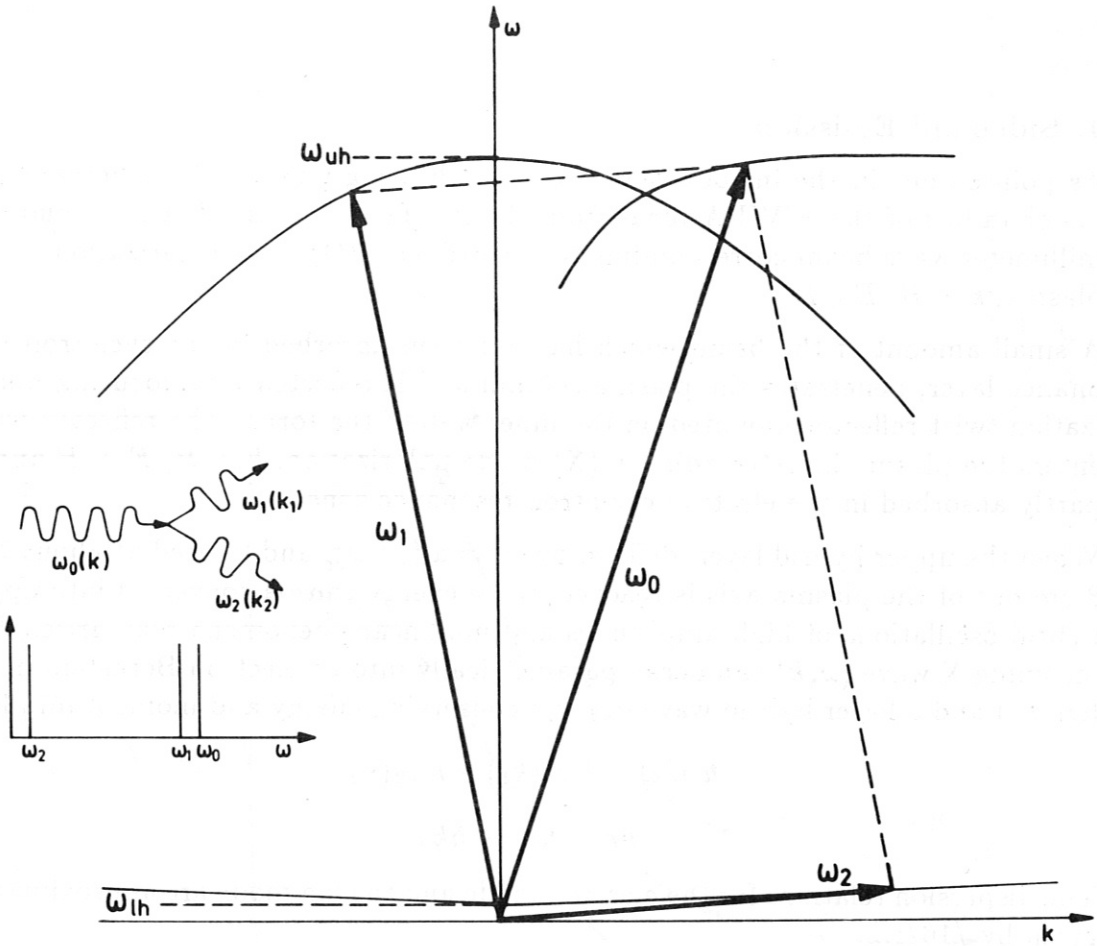

Fig. 8 The parallelogram construction demonstrates the ω-k matching in the wave decay. ω_0 is the incident X-mode wave, ω_1 and ω_2 are the decay waves.

Both sidebands to ω and the lower hybrid band around ω_{lh} have been found in the WVII-A experiment /19/. On the Versator II tokamak in addition to the low frequency band close to ω_1 its 2^{nd} harmonic has also been observed /16/.

On WVII-A sidebands to the 2^{nd} harmonic of the pump wave have been detected. They occur as additional signal power to the ECE power as measured in channel 4 and 5, and they are distinguished from the ECE by their fast decay after the gyrotron is switched off, as shown in Fig. 7 for channel 5. By scanning the band around 2ω it is found that the sidebands extend to about $-500\ MHz$ and $+350\ MHz$. The ratio of maximum power measured in the lower and upper sideband is about 6. The absolute power detected is of the same order of magnitude of the ECE power, which is about $5 \cdot 10^{-8}\ W$ per 300 MHz observation bandwidth.

The lower hybrid wave is resonant with plasma ions. It has been suggested that the occurence of an additional high energetic component in the energy distribution of the ions is due to effective coupling to the lower hybrid wave.

Estimations based on energy arguments show that some per cent of the total

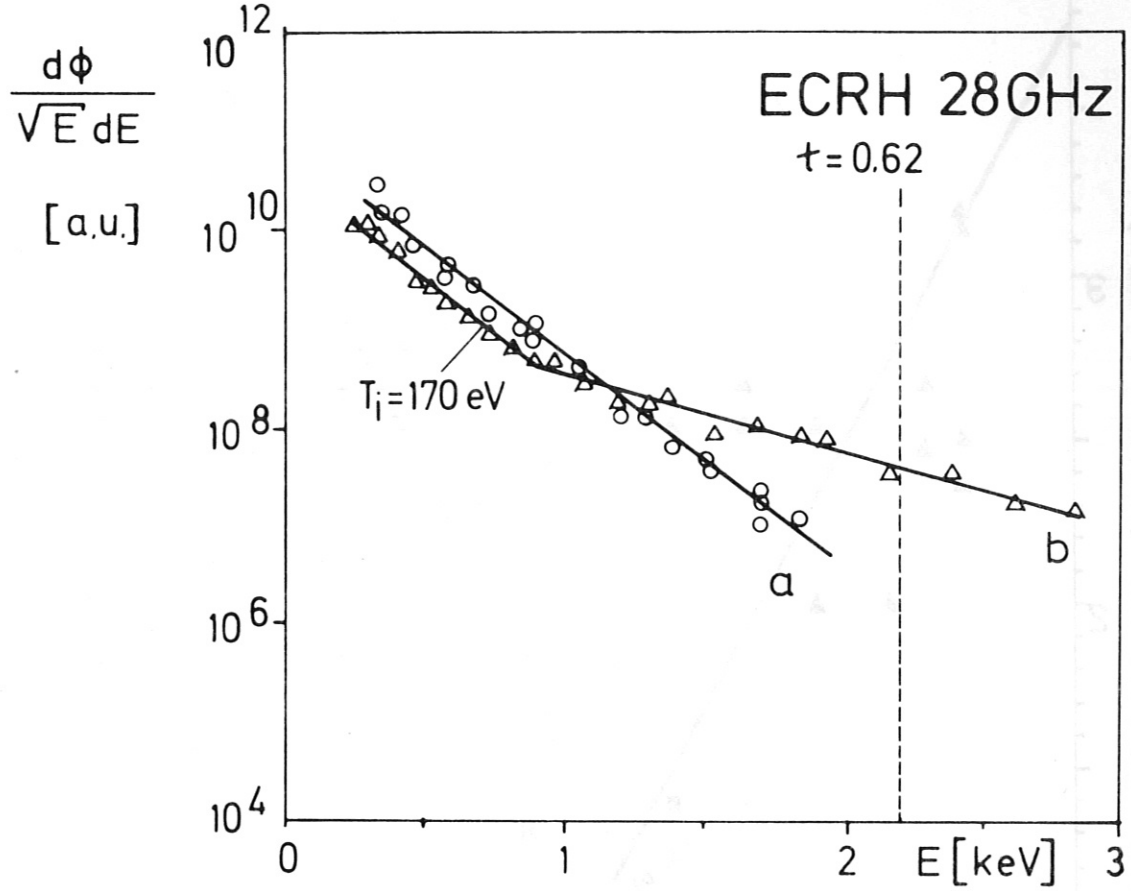

Fig. 9 Energy distribution of plasma ions as measured via charge exchange analysis for two situations: without (a) and with (b) fast tail contribution. The flux at 2.2 KeV (dashed line) is taken as measure of the correlations given in Figs. 10 and 11.

number of ions can indeed be heated up to 500 eV (as experimentally observed) whilst the bulk temperature is only about 150 eV, Fig. 9.

A clear correlation was found between the occurrence of the fast ion tail and the reflected power at the polarization twist reflector which is proportional to the X-mode power. The same correlation holds for the lower sideband power around $2\omega_1$ (channel 5). The X-mode pump power is correlated with high power at the lower sideband and large fluxes of high energetic neutrals produced with charge exchange.

In Fig. 10a the flux of 2.2 KeV neutrals is taken as a measure of the high energetic tail in the ion distribution function and is plotted as function of line density, which mainly determines the X-mode power.

Above the value of $6 \cdot 10^{13}\ cm^{-2}$ of the line density, which corresponds to about $5 \cdot 10^{18}\ m^{-3}$ central electron density, the high energy component disappears com-

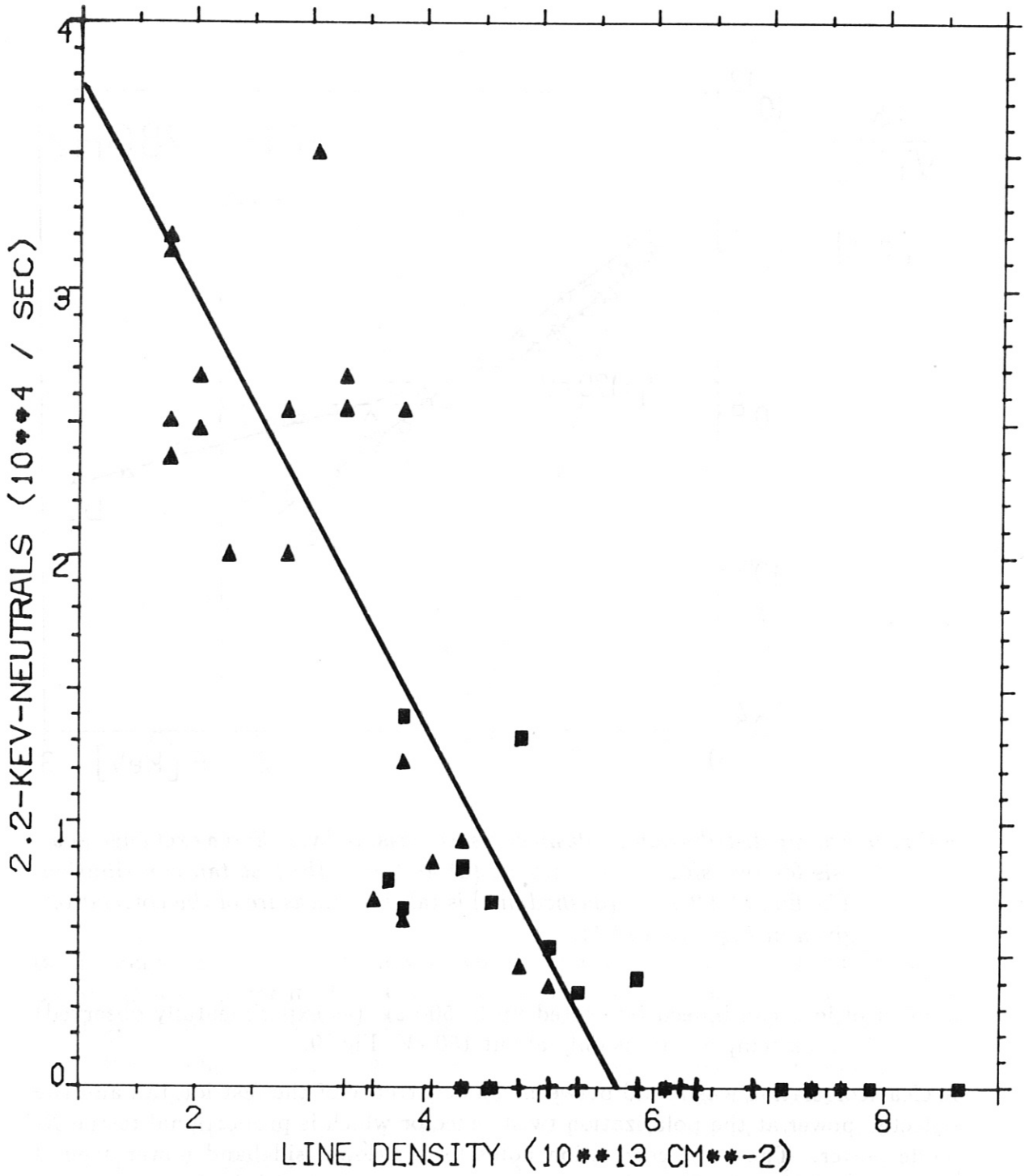

Fig. 10a 2.2 KeV neutral flux as function of line density.

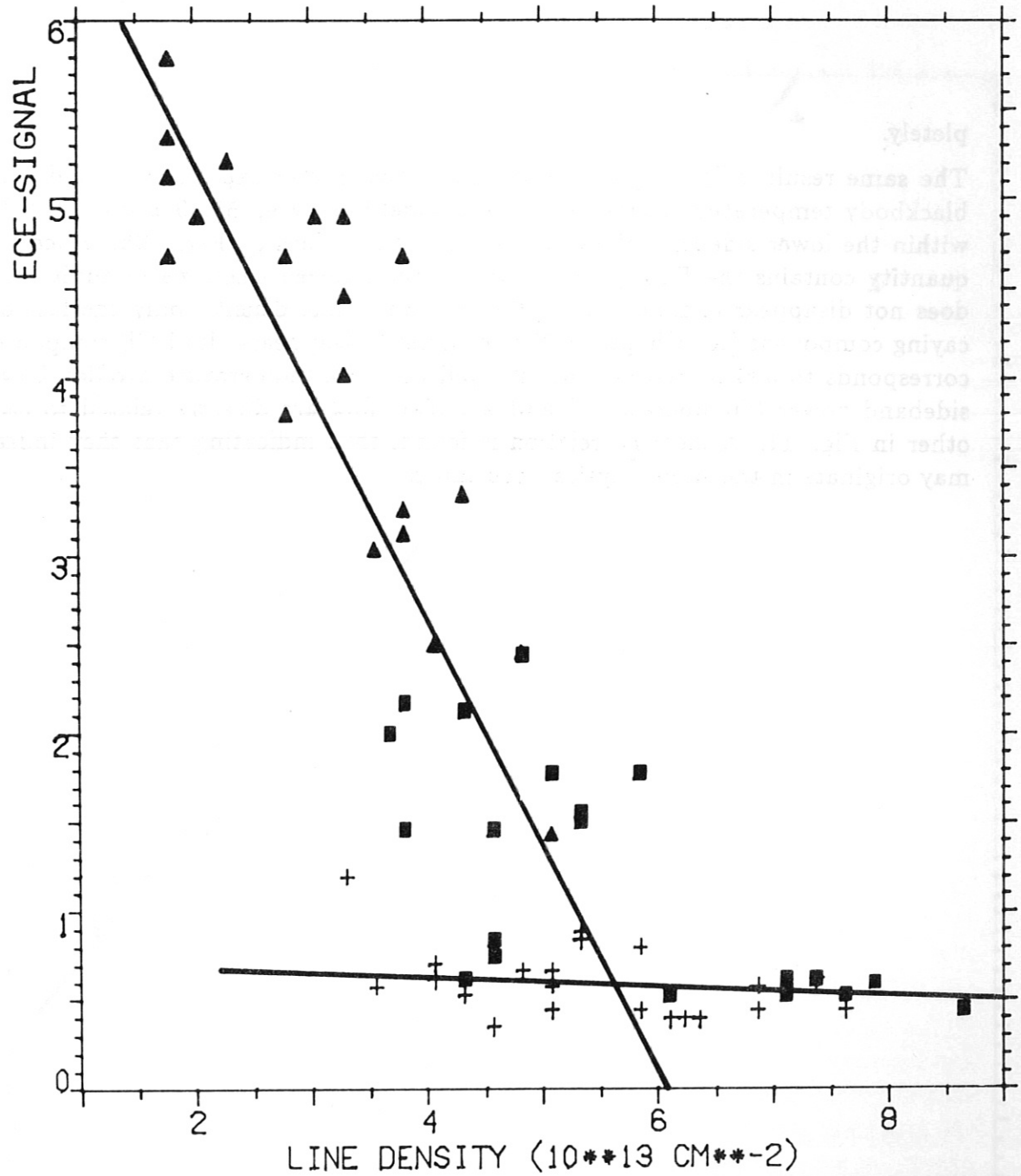

Fig. 10b ECE power in terms of equivalent blackbody temperature, as measured by channel 5 at the lower sideband of the 2^{nd} harmonic of the gyrotron radiation, is shown as function of the line density.

pletely.

The same result is found plotting the integrated power expressed in equivalent blackbody temperature as measured by channel 5 between 55.49 and 55.79 GHz within the lower sideband of 2ω as function of line density, Fig. 10b. Since this quantity contains the ECE power from the thermalized electrons in addition, it does not disappear completely. At $6 \cdot 10^{13}\ cm^{-2}$ line density, only the fast decaying component (see Chapter 3.3) of channel 5 disappears. Its ECE component corresponds to 500 to 700 eV and fits well the bulk temperature profile. Lower sideband power ("temperature") and 2.2 KeV flux are directly related to each other in Fig. 11. A clear correlation is found, thus indicating that they indeed may originate in the same physical mechanism.

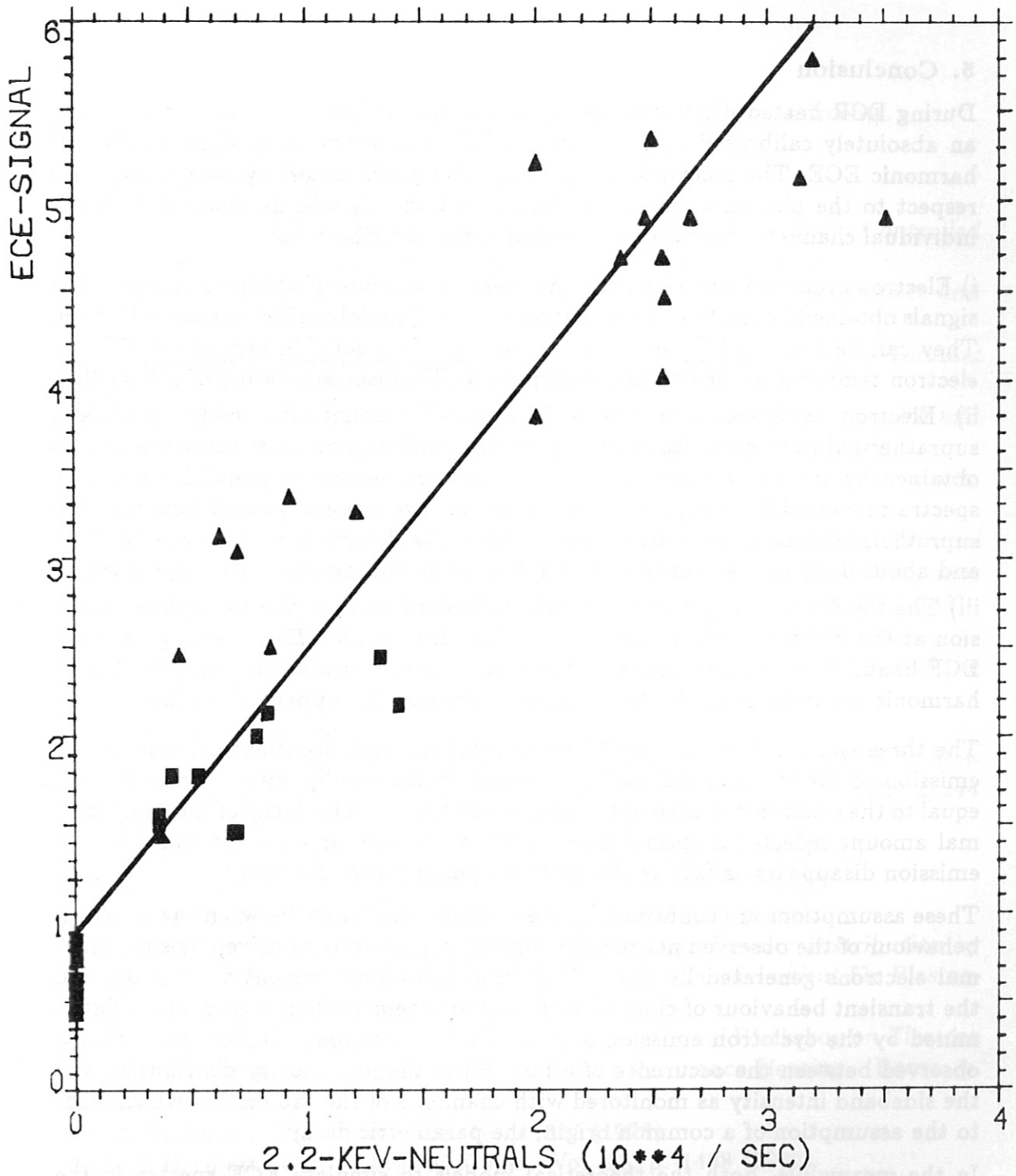

Fig. 11 Direct correlation of lower sideband power and CX-flux.

5. Conclusion

During ECR heated discharges, ECE measurements have been carried out using an absolutely calibrated eight channel radiometer, which is sensitive to the 2^{nd} harmonic ECE. The receiving channels are staggered almost symmetrically with respect to the plasma axis. It was found that the signals, as monitored by the individual channels, are superpositions of three contributions:

i) Electron cyclotron emission from the thermalized bulk of plasma electrons. The signals obtained by the four inner channels ($r_i < 0$) mainly reflect this contribution. They can be evaluated for electron temperature in resonable agreement with the electron temperature profile as determined by Thomson scattering of a laser line.

ii) Electron cyclotron emission from a small amount of weakly relativistic suprathermal electrons. Radiation from this contribution dominates the signals obtained by the outer channels ($r_i > 0$). By comparison to simulated emission spectra converted to "temperature profiles", the average energy and density of the suprathermal component can approximatively be determined to be $5 \div 15$ KeV and about 0.3% of the central electron density of the thermal bulk respectively

iii) The third contribution of completely different nature is due to sideband emission at the 2^{nd} harmonic of the gyrotron line around 56 GHz superimposing the ECE band. A possible generation process may be the parametric decay (including harmonic generation) of the X-mode pump wave at the upper hybrid layer.

The three contributions can well be separated by their transient behaviour: the emission of the thermalized electrons decays exponentially with a time constant equal to the electron confinement time of 1.5 to 1.8 ms. The decay of the suprathermal amount reflects its special slowing down and loss process and the sideband emission disappears as fast as the gyrotron pump power decreases.

These assumptions are confirmed by the complete similarity between the transient behaviour of the observed net plasma current, aspected to be driven by suprathermal electrons generated by the ECRH itself (no ohmic current is present), and the transient behaviour of channel 8 of the radiometer, which is completely determined by the cyclotron emission of suprathermal electrons. Direct correlation is observed between the occurence of a fast tail in the ion velocity distribution and the sideband intensity as monitored with channel 5 of the radiometer which leads to the assumption of a common origin, the parametric decay.

In the meanwhile, both the theoretical models to simulate ECE spectra in the presence of a suprathermal component (3-D ray tracing code) and the experimental set up have been improved and applied to 70 GHz ECRH studies. The results are in qualitative agreement with those reported here /20/.

Acknowledgement

We thank Mr. W. Breitel for technical assistence during the experiments.

References

/1/ WVII-A Team, *Proc. of the* 6^{th} *Int. Conf. on Plasma Physics and Controlled Nuclear Fusion Research, Berchtesgaden*, Vol. II, p. 81 (1976)

/2/ WVII-A Team et al., *Proc. of the* 10^{th} *Int. Conf. on Plasma Physics and Controlled Nuclear Fusion Research, London*, Vol. II, p. 371 (1984)

/3/ V. Erckmann et al., *Proc. of the* 4^{th} *Int. Symposium on Heating in Toroidal Devices, Rome*, Vol. II, p. 846 (1984)
V. Erckmann et al., *Proc. of the* 10^{th} *Int. Conf. on Plasma Physics and Controlled Nuclear Fusion Research, London*, Vol. II, p. 419 (1984)

/4/ V. Erckmann et al., *Plasma Physics and Controlled Nuclear Fusion Research*, Vol. 28, p. 1277 (1986)

/5/ H.J. Hartfuß M. Tutter, WVII-A Team, *Proc. of the 5th International Workshop on Electron Cyclotron Emission and Electron Cyclotron Resonance Heating*, San Diego, GA Technologies Document GA-A18294, p. 37 (1985)

/6/ J.Junker, M. Kick, *private communication*

/7/ O. Vollmer et al., *Aktive Neutralteilchendiagnostik am WVII, Report of the Max-Planck-Institut für Plasmaphysik*, IPP 4/172 (1978)

/8/ S. Marlier, H. Ringler, *private communication*

/9/ A. Cavallo, M. Tutter, *Electron Cyclotron Measurements in the WVII-A Stellarator, Report of the Max-Planck-Institut für Plasmaphysik*, IPP 2/244 (1978)

/10/ H.J. Hartfuß, M. Tutter, *Rev. Sci. Instr.* Vol. 56, p. 1703 (1985)

/11/ F. Engelmann, M. Curatolo, *Nucl. Fus.* Vol. 13, p. 497 (1973)

/12/ G. Bekefi, *Radiation Processes in Plasmas*, New York (1966)

/13/ M. Tutter, *A Method to measure the Suprathermal Density Distribution by Electron Cyclotron Emission, Report of the Max-Planck-Institut für Plasmaphysik*, IPP 2/244 (1986)

/14/ M. Tutter, H.J. Hartfuß, *Proc. of the* 4^{th} *International Workshop on Electron Cyclotron Emission and Electron Cyclotron Resonance Heating*, Roma, p. 167 (1984)

/15/ M. Porkolab, *Nucl. Fus.* Vol. 18, p. 367 (1978)

/16/ F.S. Dermott et al., *Phys. of Fluids*, Vol. 25, p. 1488 (1982)

/17/ J.A.Ratcliffe, *The Magneto-Ionic Theory and its Application to the Ionosphere*, Cambridge (1962)

/18/ M. Porkolab, R.P.H. Chang, *Rev. Mod. Phys.* Vol. 50, p. 745 (1978)

/19/ V. Erckmann et al., *Fusion Technology*, Vol. 7, p. 275 (1985)

/20/ H.J. Hartfuß et al. *Proc. of the 5th International Workshop on Electron Cyclotron Emission and Electron Cyclotron Resonance Heating*, Oxford (1987), (to be published).